

Automatic Recognition and Modeling of Piping System from Large-scale Terrestrial Laser Scanned Point Cloud

Kazuaki Kawashima, Satoshi Kanai² Hiroaki Date³ Tae-wan Kim⁴

^{1,2,3} Graduate School of Information Science and Technology, Hokkaido University, Japan,

k_kawashima@sdm.ssi.ist.hokudai.ac.jp, (kanai, hdate)@ssi.ist.hokudai.ac.jp

⁴ Department of Naval Architecture and Ocean Engineering, Seoul National University, Korea,

taewan@snu.ac.kr

Abstract:

In recent years, constructing 3D as-built models of existing plants from large-scale laser scanned data has been expected to make rebuilding processes more efficient. However, laser scanned data consists of a massive number of points and includes a high noise level, so that the manual reconstruction of a 3D model is very time-consuming. Among plant equipment, piping systems especially account for the greatest proportion. Therefore, the purpose of this research was to propose an algorithm which can automatically recognize a piping system from terrestrial laser scan data of plants. The straight portion of pipes, connecting parts and connection relationship of the piping system can be automatically recognized. Normal-based region-growing can extract points of the piping system. Eigen analysis of the normal tensor and cylinder surface fitting allows for the recognition of portions of straight pipes. Tracing the axes of the piping system can derive connecting parts and connection relationships between elements of the piping system. The algorithm was applied to large-scale scanned data of an oil rig and an air-condition machine room. The results of the recognition rate of straight pipes, elbows, junctions were achieved at 87%, 77% and 75% respectively.

Keywords: Laser scanning, Object recognition, Point clouds, As-built model, Piping system, Normal tensor

1. Introduction

In recent years, changes in plant equipment have been frequent because the life cycles of its products are becoming short. However, the changes are not necessarily recorded in the plant drawings. Thus, unintended collisions between existing equipment and new ones often occur in the construction stage.

On the other hand, because of advances of terrestrial laser scanner performance, massive point clouds of real environments can be obtained very easily and quickly. Also, as-built modeling from laser scanned point clouds is expected to make the plant reconstruction process more efficient. Once the models are reconstructed, the unintended collisions can be avoided before construction.

However, the laser scanned data of existing plants have massive points, and include a high noise level. Therefore, recognizing each plant component from the scanned data and building 3D models of the plants are nearly impossible or very time consuming when done manually. Thus, automatic recognition and construction of 3D models from point clouds needs to be strongly encouraged in the plant engineering field.

Plants consist of many types of components. Among them, the piping systems especially account for the greatest proportion and are renovated frequently. As shown in Fig.1, a piping system consists of various piping elements and connection relationships; straight pipes, connecting parts such as junctions and elbows, and attached parts such as indicators, etc. Also, the connection relationship defines the logical connectivity

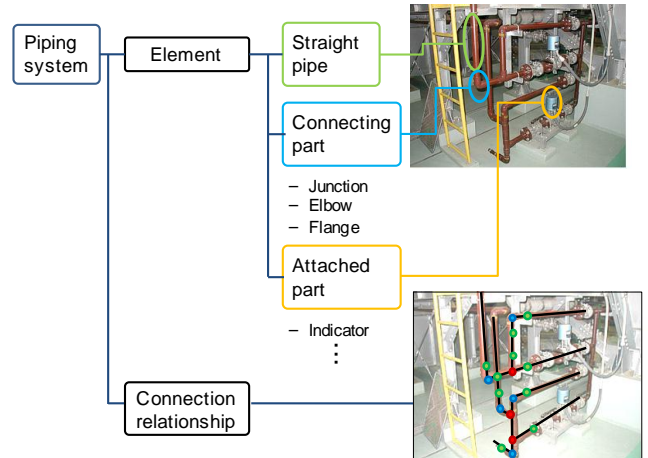


Figure.1 Elements of piping system

between these piping elements.

Several studies have been proposed to recognize a piping system from a laser scanned point cloud [2,3,4,5,6]. However, these algorithms cannot recognize pipes in a fully automatic way, or cannot be directly applied to a registered point cloud. Moreover, there are also some studies to extract piping objects from scanned points of outdoor environments. However, they could not explicitly estimate the radii and length of objects and are not useful for plant engineering.

Therefore, the purpose of our research was to propose a new algorithm that can automatically recognize piping

elements and their connection relationships from a registered laser scanned point cloud of a plant. In addition, the algorithm can recognize defining parameters of straight pipes, elbows and junctions with high accuracy.

The algorithm was tested for large-scale laser scanned point clouds of real plants, and the accuracies of recognition of the straight pipes and connecting parts were verified.

We have already proposed a piping system recognition algorithm [1]. However, it had some problems; scanned points on the plant components other than the piping system should be removed in advance, recognition rates of connecting parts are less than 50%, and the algorithm needs about 2 hours to calculate the normal vector and normal tensor for scanned data with 4,500,000 points. In this paper, we solve these problems by; 1) introducing normal-based region-growing which automates the removal of the points other than the piping system, 2) tracing axes of the piping system and fitting line-arc segments to the axes to improve the recognition rates, and 3) we interlace the normal calculation only at decimated points to reduce their calculation time. Thanks to these methods, we achieved significant improvement in recognition rates of connecting parts and calculation time compared to [1].

2. Related works

So far, several studies have been done to recognize objects from laser scanned data of plant equipment.

Masuda et al. [2] proposed a method which can recognize planes and cylinders from scanned data of plants. However, a region to be recognized has to be selected manually in advance. Ikeda et al. [3] also proposed a method similar to [2], but it requires the combination of a measured point cloud, a range image and a reflection intensity image.

Rabbani et al. [4] also proposed a method which reconstructs a 3D plant model from the combination of point cloud data and a photo taken from a single measuring location. However, their method can only be applied to the combination of a point cloud and an image generated by a single scan. Piping systems usually occupy a large-space in plants, and multiple scans must be taken and each be registered to obtain a point cloud which can cover the existing space of the whole of the piping system. Unfortunately, it is hard for the method to be applied to a huge point cloud which is created by the registration of points generated by multiple scans.

Aurelien et al. [5] also proposed a method which fits cylinder models to the scanned data of plants using a priori CAD models. However, the cylinder models whose radii and length are similar to those of pipes should be placed near points on pipes in advance.

Andrew et al. [6] proposed a method which can semi-automatically build a 3D model by matching a point cloud to a CAD model using spin image. However, the matching is inefficient because it uses an exhaustive search, and an experimental verification was not done.

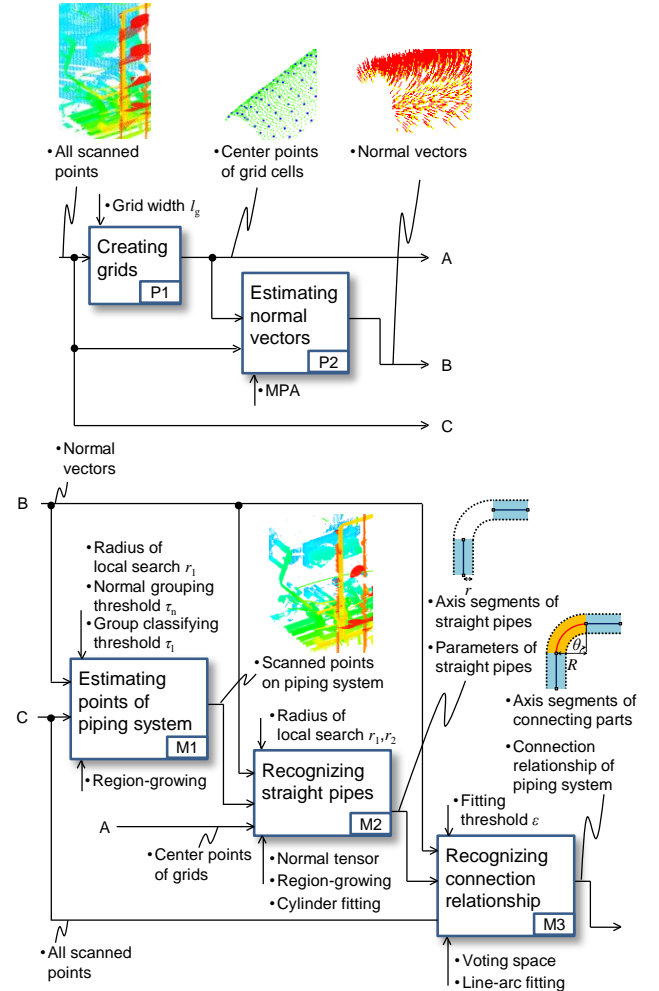


Figure.2 Process of the proposed piping system recognition

Moreover, there are some studies to extract piping objects from laser scanned data of outdoor environments. Yan et al. [7] and Alexander et al. [8] proposed a skeletonization algorithm which classifies the scanned point cloud into several groups, each of which corresponds to a single skeleton. Their algorithm can be used to recognize the axes of a piping system and connection relationship in the system. However, it is hard for this algorithm to recognize straight pipes and connecting parts from the point cloud of a plant.

3 Algorithm overview

As shown in Fig.2, our algorithm consists of two preprocesses and three main processes.

In the preprocess steps, at first, grids are positioned in whole scanned environment. All scanned points are assigned to one of the grid cells. Then, for each grid, a parabolic surface is fitted to scanned points in the grid cell, and normal vectors of the points are calculated from the surface.

In main process steps, at first, only the points on the piping system are extracted using normal-based region-growing. Next, points on straight pipes are extracted by normal tensor and region-growing, and cylinders are finally fitted to the points. The radii and positions of the cylinders are determined as the defining

parameters of straight pipes. Then, tracing axes of the piping system from the recognized straight pipes can recognize the axes of connecting parts and connection relationships between the elements of the piping system, and the defining parameters of connecting parts are recognized from the axes of the piping system.

4 Preprocessing

4.1 Creating grids (P1)

In order to increase in speed of calculating normal vectors and normal tensors, grids which have a width, w , are placed to cover whole scanned space. Each grid cell keeps up scanned points in the grid cell. If w becomes larger, scanned points on whole circumference of a pipe could be included in a cell and in its one-neighbor 26 grid cells. As a result, irrelevant surface is fitted to the points and inaccurate normal vectors are estimated at the points in the process of estimating normal vectors (P2). Thus, w was set as one third of the smallest pipe radius in the space, r_{\min} , in this paper.

4.2 Estimating normal vectors (P2)

In order to estimate normal vectors of all scanned points, for each grid cell, a parabolic surface, S , is fitted to the points in the cell and its one-neighbor 26 grid cells $\{\mathbf{p}_j\}$ according to the moving parabolic approximation proposed in [9].

Let \mathbf{X} denote a center point of the grid, and \mathbf{O}_x denote a footprint of \mathbf{X} on the surface, S . Then, we can define a local orthogonal system $\mathbf{O}_x - \mathbf{u} - \mathbf{v} - \mathbf{n}$ where \mathbf{n} is a normal vector, \mathbf{O}_x , on the surface, S , and vectors $\mathbf{u}(\mathbf{n})$ and $\mathbf{v}(\mathbf{n})$ are perpendicular to the vector \mathbf{n} . Then, in the system, a height from a tangential plane which passes through \mathbf{O}_x to a scanned point, \mathbf{p}_j is expressed as $h_j = (\mathbf{p}_j - \mathbf{O}_x)^T \mathbf{n}$, and u-v parameters in the system are expressed as $u_j = (\mathbf{p}_j - \mathbf{O}_x)^T \mathbf{u}(\mathbf{n})$, and $v_j = (\mathbf{p}_j - \mathbf{O}_x)^T \mathbf{v}(\mathbf{n})$. If we determine the coordinate values in uvn axis directions as (u, v, w) , a parabolic surface $w(u, v) = 1/2(au^2 + 2buv + cv^2)$, which is fitted to scanned points in the neighboring grid cells, is expressed as equation (1):

$$\min_{a,b,c} \sum_{j=1}^n \left[h_j - \frac{1}{2}(au_j^2 + 2bu_jv_j + cv_j^2) \right]^2 \theta(\|\mathbf{p}_j - \mathbf{O}_x\|) \\ \theta(d) = e^{-d^2/\rho^2} \quad (1)$$

where $\theta(d)$ is a weight function, ρ is a scale parameter and n is the number of points in the grid cell and its one-neighbor 26 grid cells. Then, equation (1) can be rewritten to a constrained optimization problem (2) when substituting $\mathbf{q}_j = \mathbf{p}_j - \mathbf{X}$, $\mathbf{O}_x = \mathbf{X} + \zeta \mathbf{n}$

$$\min_{a,b,c} f(\mathbf{n}, \zeta, a, b, c) = \min_{a,b,c} \sum_{j=1}^n \left[\mathbf{q}_j^T \mathbf{n} - \zeta - \frac{1}{2} \{ a(\mathbf{q}_j^T \mathbf{u}(\mathbf{n}))^2 \right. \\ \left. + 2b(\mathbf{q}_j^T \mathbf{u}(\mathbf{n}) \mathbf{q}_j^T \mathbf{v}(\mathbf{n}) + c(\mathbf{q}_j^T \mathbf{v}(\mathbf{n}))^2 \} \right]^2 e^{-\frac{\|\mathbf{q}_j - \zeta\|^2}{\rho^2}}$$

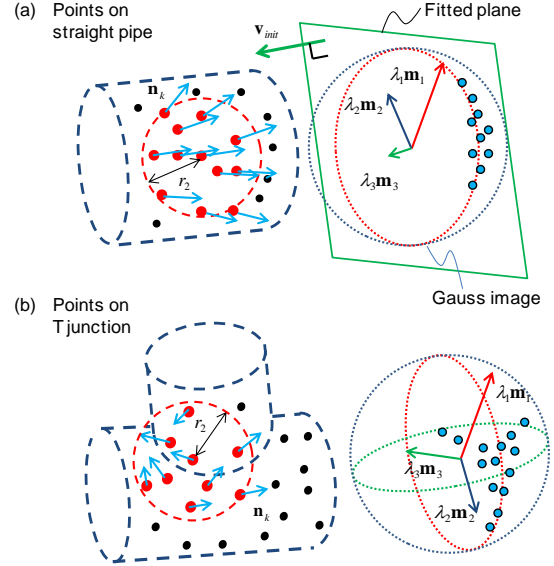


Figure 3 Normal gauss image and eigenvectors of normal tensor

$$\text{s.t. } \mathbf{n}^T \mathbf{n} - 1 = 0 \quad (2)$$

The optimization problem was solved by the Newton-Raphson method. Then, the scanned points in the grid cells are projected to the surface, S , and the normal vector at the projected point finally becomes a normal vector, \mathbf{n}_j , of \mathbf{p}_j .

5 Extracting points of a piping system (M1)

After calculating normal vectors, points on the piping system are extracted from all scanned points, P , by applying normal based region-growing.

First, a seed point, $\mathbf{p}_s \in P$, of a region is chosen from all scanned points at random. Then, the points $\{\mathbf{p}_i | \mathbf{p}_i \in P, \mathbf{p}_i \in N(\mathbf{p}_s, r_1), \|\mathbf{n}_s \cdot \mathbf{n}_i\| > \tau_n\}$ where $N(\mathbf{p}_s, r_1)$ is a set of neighboring scanned points contained in the sphere of the radius, r_1 , centered at \mathbf{p}_s are added to the region. τ_n was set to be 0.98 in this paper. Each of the added points is then chosen as a new seed point, and the other points satisfying the same condition are added to the region. The above steps are repeated until the points satisfying the condition exist in the neighborhood of the seed points. Then, the points in the region are projected to a plane whose normal vector is \mathbf{n}_s , and an oriented bounding box of the projected points is calculated. If the scanned points exist on curved surfaces such as pipes, the smaller width of the bounding box, l , becomes very small. While the points exist on planar surfaces such as floors or walls, l becomes larger than that of the former case. Thus, if the width of l satisfies $l < \tau_l$ where τ_l is a threshold to l , the points in the region are classified as points on the piping system. Otherwise, they are classified as points on the other components. τ_l was set equal to the smallest pipe radius in the scanned space.

6 Recognizing straight pipes (M2)

6.1 Extracting points on straight pipes

First, the normal tensor, T_i , is evaluated for a set of points, $N(\mathbf{g}_i, r_2)$, by equation (3), where \mathbf{g}_i is the center point of the grid cell [10].

$$T_i = \frac{1}{|N(\mathbf{g}_i, r_2)|} \sum_{j \in N(\mathbf{g}_i, r_2)} \mathbf{n}_j^T \cdot \mathbf{n}_j \quad (3)$$

where \mathbf{n}_j is the normal vector of scanned point, \mathbf{p}_j .

Then, the eigenvalues, $\lambda_1, \lambda_2, \lambda_3$ ($\lambda_1 \geq \lambda_2 \geq \lambda_3 \geq 0$), and corresponding eigenvectors, $\mathbf{m}_1, \mathbf{m}_2, \mathbf{m}_3$, are evaluated by eigen analysis of T_i . The smallest eigenvalue, λ_3 , of T_i is assigned to all scanned points in the grid cell. These eigenvalues and eigenvectors show spatial distributions of the normal gauss image, as shown in Fig.3. For example, at a point \mathbf{g}_i is close to a straight portion of pipe, the normal vectors in $N(\mathbf{g}_i, r_2)$ exist almost on one plane. Then, λ_3 becomes much smaller than λ_1 and λ_2 . When \mathbf{g}_i is close to an elbow or a junction, the normal vectors are distributed three-dimensionally. Then, λ_3 becomes larger than that of the former case. Thus, limiting $\lambda_3 \leq \tau_i$ enables the points to be classified into the points on straight pipes and those on other elements such as elbows and junctions. This relevant threshold value for τ_i is determined by the discriminant analysis method [11].

6.2 Grouping points on a straight pipe

After classifying points into the ones on the straight pipes, the points on one straight pipe are furthermore integrated into a single region using the region-growing method.

First, a seed point, \mathbf{p}_s , is chosen from the classified points on the straight pipes at random. Then, the other points on the straight pipes contained in neighboring points $N(\mathbf{p}_s, r_1)$ centered at \mathbf{p}_s are added into the region. Each of the added points is next chosen as a new seed point, and the above step is repeated similarly until points on the straight pipes exist in the neighborhood of the seed points.

6.3 Extracting initial pipe parameters

After grouping points on the straight pipes, cylinders are fitted to the groups and the axes of the pipes and their radii and length are estimated.

First, a normal gauss image is created from all points in a region. Then, a plane is fitted to the gauss image using RANSAC, and an initial axis vector, \mathbf{v}_{init} , is obtained as the normal vector of the plane. In the RANSAC, the sampling number is 500, and the outlier threshold to the inner product of normal vectors is set as 0.01 in this paper. Then, all points in the region are projected to the plane, and a circle is fitted to the projected points by the least-square method. The center point and the radius of the fitted circle are respectively taken as an initial point on an axis, \mathbf{s}_{init} , and an initial radius, r_{init} , of the pipe.

Then, a cylinder is precisely fitted to the points of the

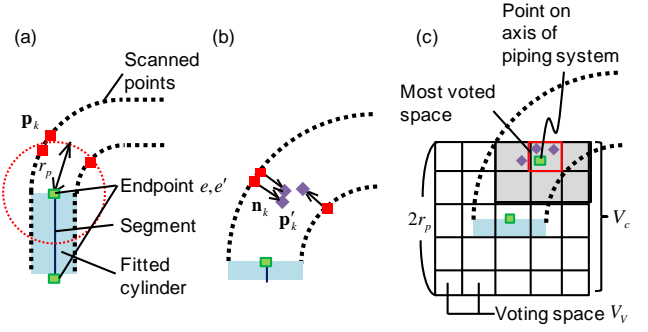


Figure.4 Tracing points on axis of piping system

Algorithm.1 Fitting line-arc segments

Require: A sequence of axis points $[\mathbf{d}_1, \mathbf{d}_2, \dots, \mathbf{d}_n]$ and a tolerance value ε
Ensure: Line-arc segments $[l'_1, a'_1, l'_2, a'_2, \dots, l'_m]$ approximating $[\mathbf{d}_1, \mathbf{d}_2, \dots, \mathbf{d}_n]$ with distance at most ε to each axis point \mathbf{d}_i

```

i = 1 ; count = 1
while i < (n - 1) do
  for all j > i do
    let  $Q$  be the plane spanned by  $\mathbf{d}_i, \mathbf{d}_{i+1}, \mathbf{d}_{j+1}$ 
    for all  $\mathbf{d}_k \in \{\mathbf{d}_i, \mathbf{d}_{i+1}, \dots, \mathbf{d}_{j+1}\}$  do
      let  $\mathbf{d}'_k$  be the point  $\mathbf{d}_k$  projected onto  $Q$ 
       $\varepsilon'_k = \sqrt{\varepsilon^2 - \|\mathbf{d}'_k - \mathbf{d}_k\|^2}$ 
    end for
     $l_1 = \mathbf{d}'_i \mathbf{d}'_{i+1}$  ;  $l_2 = \mathbf{d}'_j \mathbf{d}'_{j+1}$  ;  $\mathbf{L} = l_1 \cap l_2$ 
    for all  $\mathbf{d}'_k \in \{\mathbf{d}'_{i+1}, \mathbf{d}'_{i+2}, \dots, \mathbf{d}'_j\}$  do
      solve LLP problem to:  $l_1, l_2, \mathbf{d}'_k$ 
      if there are solutions then
        let  $\mathbf{c}$  be the circle center farthest from  $\mathbf{L}$  and
         $\mathbf{M}_1, \mathbf{M}_2$  be projection of the circle onto  $l_1$  and
         $l_2$ 
        for all  $\mathbf{d}'_l \in \{\mathbf{d}'_{i+1}, \mathbf{d}'_{i+2}, \dots, \mathbf{d}'_j\}$  do
          let  $s'_l$  be smallest distance between  $\mathbf{d}'_l$  and
          segments  $\mathbf{d}'_i \mathbf{M}_1, \mathbf{M}_1 \mathbf{d}'_{j+1}, \mathbf{M}_1 \mathbf{M}_2$ 
          if all  $\mathbf{d}'_l \in \{\mathbf{d}'_{i+1}, \mathbf{d}'_{i+2}, \dots, \mathbf{d}'_j\}$  satisfy  $s'_l \leq \varepsilon'_l$ 
          then
             $l'_{count} = \overline{\mathbf{d}'_i \mathbf{M}_1}, a'_{count} = \overline{\mathbf{M}_1 \mathbf{M}_2}$ 
             $j_{save} = j$ 
             $\mathbf{d}_{save} = \mathbf{M}_2$ 
          end if
        end for
      end if
    end for
  end if
end for
if  $j_{save} = n - 1$  then
   $l'_{count+1} = \overline{\mathbf{M}_2 \mathbf{d}'_n}$ 
else
   $i = j_{save}$ 
   $\mathbf{d}_i = \mathbf{d}_{save}$ 
  count = count + 1
end if
while end

```

region using the non-linear least square method [12]. In this method, if we express the parameters of the cylinder as $(f, g, h, \alpha, \beta, \gamma, r)$, where (f, g, h) is the components of the pipe axis vector, \mathbf{v} , (α, β, γ) the components of a position vector, \mathbf{s} , of a point on the axis, and r the radius of the cylinder, then an objective function of the fitting is expressed in equations (4), (5) and (6):

$$\frac{1}{N} \sum_{i=0}^{N-1} (f_i - r)^2 \quad (4)$$

$$f_i = \sqrt{m^2 + n^2 + o^2} \quad (5)$$

$$\begin{aligned} m &= h(y_i - \beta) - g(z_i - \gamma) \\ n &= f(z_i - \gamma) - h(x_i - \alpha) \\ o &= g(x_i - \alpha) - f(y_i - \beta) \end{aligned} \quad (6)$$

where (x_i, y_i, z_i) is a position vector of the point in the region and N is number of the points in the region.

Then, the fitted cylinders whose radii, r , and average fitting error, $\bar{\varepsilon}$, exceed their allowable range $(\bar{\varepsilon} < \varepsilon_r) \wedge (r > r_{\min}) \wedge (r < r_{\max})$ are ignored in the recognition where r_{\max} is the largest pipe radius in the scanned space.

Finally, the remaining points in the region are projected to the cylinder axis, and two endpoints of the projected points on the axis are taken as endpoints, \mathbf{e} and \mathbf{e}' , as shown in Fig.4-(a). The line segment, \mathbf{ee}' , is further used for recognizing connection relationships among pipes.

7 Recognizing connection relationship (M3)

In order to further discover unrecognized straight pipes and connecting parts, the connection relationships between the elements of the piping system are estimated by tracing the axis segments generated in section 6.3 and the scanned points.

7.1 Tracing points on axes of a piping system

Shown in Fig.4, first, a sphere is centered at one of the endpoints, \mathbf{e}_i , and scanned points, $\{\mathbf{p}_k\}$, nearly existing on the sphere are collected from all scanned points. The radius of the sphere, r_p , is set as $1.1r$ where r is the radius of the fitted cylinder. Then, a set of offset points, $\{\mathbf{p}'_k\}$, is generated from $\{\mathbf{p}_k\}$ as $\mathbf{p}'_k = \mathbf{p}_k + r_p \mathbf{n}_k$, where \mathbf{n}_k is a normal vector towards the inside of the fitted cylinder. Then, a cube space, V_c , with the length $2r_p$, where the center point is at \mathbf{e}_i , is placed. Then, V_c is uniformly partitioned into a set of small voting spaces, V_v . Then, each offset point, \mathbf{p}'_k , is voted for V_v . If the number of the vote in the most voted space and its-one neighboring 26 spaces exceeds half the number of points, \mathbf{p}'_k , an axis point, \mathbf{d} , is estimated as at an average position of the points included in the 27 spaces.

The above steps are repeated until scanned points exist on the sphere and satisfy the voting condition, and the axis points $[\mathbf{d}_1, \mathbf{d}_2, \dots, \mathbf{d}_n]$ are finally obtained.

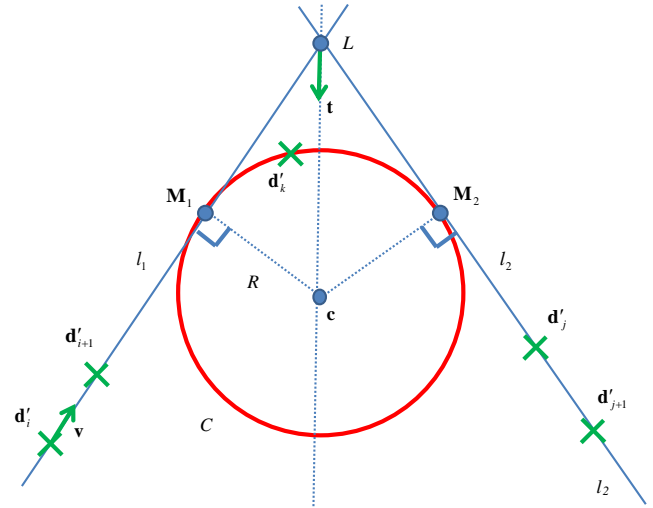


Figure 5 Fitting line-arc segments

7.2 Fitting line-arc segments to the axis points

After recognizing the axis points of a piping system, a line or an arc segment is alternately fitted to these points [13], so that the distance between the segments and all axis points $[\mathbf{d}_1, \mathbf{d}_2, \dots, \mathbf{d}_n]$ becomes less than a threshold, ε . The ε was set as $0.1r$ in this paper.

Pseudocode of the algorithm is shown in Algorithm 1. As shown in Fig.5, first, a plane, Q , passing through three axis points $\mathbf{d}_i, \mathbf{d}_{i+1}, \mathbf{d}_{j+1} (i+1 < j)$ is obtained. Then, the subsequence of the axis points $[\mathbf{d}_i, \dots, \mathbf{d}_{j+1}]$ are projected to the plane. The allowable fitting error, ε'_k , between the projected axis point $\mathbf{d}'_k \in \{\mathbf{d}'_{i+1}, \mathbf{d}'_{i+2}, \dots, \mathbf{d}'_j\}$ and these segments on the plane, Q , can be shown as equation (7).

$$\varepsilon'_k = \sqrt{\varepsilon^2 - \|\mathbf{d}'_k - \mathbf{d}'_k\|} \quad (7)$$

Next, lines $l_1 = \overline{\mathbf{d}'_i \mathbf{d}'_{i+1}}$, $l_2 = \overline{\mathbf{d}'_j \mathbf{d}'_{j+1}}$ and their intersection point, \mathbf{L} , are calculated. For each projected axis point, $\mathbf{d}'_k \in \{\mathbf{d}'_{i+1}, \mathbf{d}'_{i+2}, \dots, \mathbf{d}'_j\}$, a circle, C , which is tangential to l_1 and l_2 , and passing \mathbf{d}'_k has to be found by the following method.

The tangent point, \mathbf{M}_1 , between C and l_1 satisfies equation (8).

$$R = \|\mathbf{c} - \mathbf{p}'_k\| = \|\mathbf{c} - \mathbf{M}_1\| \quad (8)$$

where \mathbf{c} is a center point of C and R radius of C . If we denote \mathbf{c} as $\mathbf{L} + \lambda \mathbf{t}$ where \mathbf{t} is a directional vector of the bisector line of l_1 and l_2 , the equations can be rewritten to equations (9) and (10):

$$(\|\mathbf{w}\|^2 - \|\mathbf{t}\|^2)\lambda^2 + 2\{(\mathbf{w} \cdot \mathbf{y}) - (\mathbf{t} \cdot \mathbf{z})\}\lambda + (\|\mathbf{y}\|^2 - \|\mathbf{z}\|^2) = 0 \quad (9)$$

$$\begin{aligned} \mathbf{w} &= \mathbf{t} - (\mathbf{t} \cdot \mathbf{v})\mathbf{v} \\ \mathbf{y} &= \mathbf{L} - \mathbf{p}'_i - \{(\mathbf{L} - \mathbf{p}'_i) \cdot \mathbf{v}\}\mathbf{v} \\ \mathbf{z} &= \mathbf{L} - \mathbf{M} \end{aligned} \quad (10)$$

where \mathbf{v} is a directional vector of l_1 . The larger solution of the quadratic equation (9) gives the center point, \mathbf{c} , and the radius, R , of C . From the solution, a line segment, $l' = \mathbf{d}'_i \mathbf{M}_1$, and an arc segment,

$a' = \overline{\mathbf{M}_1 \mathbf{M}_2}$, are obtained.

If any segment is not reached to the last axis point, \mathbf{d}_n , the tangent point, \mathbf{M}_2 , between C and l_2 and \mathbf{d}'_{j+1} are treated as new axis points, and a new line and arc segment are fitted to the remaining axis points $[\mathbf{M}_2, \mathbf{d}'_{j+1}, \dots, \mathbf{d}_n]$.

However, arc segments which have very large radii are sometimes fit even for axis points of straight pipes. To correct these irrelevant fitting results, if consecutive line-arc-line segments are nearly collinear, the three segments are replaced with one line segment.

7.3 Recognizing the axes of junctions

The method shown in section 7.1, in case of the branching axis points in junctions, only a sequence of axis points which connect one port to another port can be extracted, and the axis points for the remaining ports cannot be discovered. Therefore, the undiscovered axis points at junctions are reconstructed from the known line-arc segments of known axis points. The reconstruction process falls into one of four cases, as shown in Fig.6.

As shown in step 1 in Fig.6-(a),(b), for each arc segment, two line segments connected to the arc are extended by a distance, l_d , and a cylinder whose radius is as same as the cylinder corresponding to the line segment is placed and aligned to the extended axis. l_d was set to be three times the original cylinder's radius. If scanned points do not exist inside of the cylinder, the arc segment is removed, as shown in step 2 in Fig.6-(a),(b). As shown in Fig.6-(a), for any endpoint not existing in the cylinder, the methods described in section 7.1 and 7.2 are further applied to the endpoint of the extended line segment, and the undiscovered straight pipe portion can be recognized.

On the other hand, as shown in step 1 in Fig.6-(c),(d), for each line segment, a cylinder whose radius is a bit larger than the fitted cylinder's radius is placed and aligned to the line segment. Then, the similar methods are applied to points on the cylinder surface. Then, as shown in step 2 in Fig.6-(c), if a new endpoint is discovered and no other endpoints exist in the cylinder, the similar methods are further applied to the new endpoint, and then undiscovered axis points and fitted segments can be recognized.

Next, as shown in step 3 in Fig.6, in order to connect line segments in junctions, some line segments are inserted in between the pairs of the original line segments. The step is described in detail as follows. Pairs of nearly collinear line segments, S_i and S_j , which satisfy $|\mathbf{v}_i \cdot \mathbf{v}_j| > \tau_{inner}$, are selected. Here, \mathbf{v} is a unit vector of the original line segment. The threshold, τ_{inner} , was set to be 0.98 in our experiments. Then, the segment pair whose endpoints, \mathbf{e}_i and \mathbf{e}_j , take the minimum distance is selected. If the distance is less than τ_l , a new line segment is inserted between \mathbf{e}_i and \mathbf{e}_j . Next, a pair of segments, S_k and S_l , which satisfy $|\mathbf{q}_l - \mathbf{q}_k| < \tau_{skew}$ and $|\mathbf{e}_l - \mathbf{e}'_k| > |\mathbf{q}_l - \mathbf{e}_l|$ are selected, where \mathbf{q}_k and \mathbf{q}_l are position vectors of the footprints

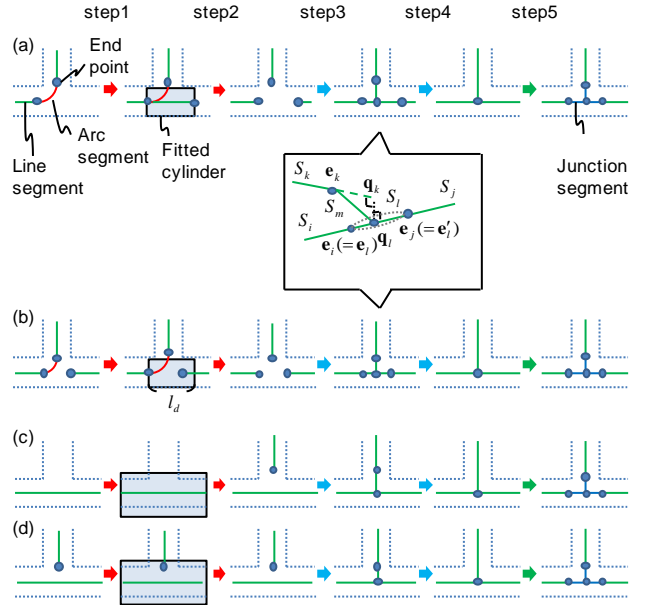


Figure.6 Recognizing axes of junction

of a common perpendicular line of two lines, L_k and L_l , each of which pass through respective endpoints \mathbf{e}_k and \mathbf{e}_l and are collinear to line segments, and τ_{skew} is the threshold for the skew distance between L_k and L_l . τ_{skew} was set to be 0.1 times the fitted cylinder's radius. Then, if the segment pair gives distance $|\mathbf{e}_k - \mathbf{q}_l|$ less than τ_l , a new line segment is inserted in between the endpoint, \mathbf{e}_k , and the intersection point, \mathbf{q}_l .

Then, as shown in steps 4 and 5 in Fig.6, line segments which are successively connected are replaced with one line segment. Then, three endpoints are inserted to line segments which connect to the junction. The distance from the junction to these endpoints was set to be identical to the fitted cylinder radius, r .

7.4 Classification of elements of a piping system

After recognition of axes of a piping system, all segments are classified to one of three classes; “straight pipe,” “elbow,” or “junction.” Line segments correspond to straight pipes. Arc segments correspond to elbows. Line segments which have an endpoint connecting three segments correspond to junctions. These classes have defining parameters of the elements of the piping system from recognized axis segments. “Straight pipe” class has a pipe radius and pipe direction. “Elbow” class has a pipe radius, bending radius and bending angle. “Junction” class has a pipe radius and angles between connecting line segments.

8 Results

As experiments of the recognition, as shown in Fig.7(a) and Fig.8(a), a large point cloud was scanned from a real oil rig by a laser scanner (Cyra Technologies CYRAX2500), and another cloud from an air-conditioning machine room by another laser scanner (Leica HDS6000). They had 4,524,324 points and 4,075,752 points, respectively. The thresholds of the oil rig

recognition were $r_1 = 20.0$, $r_2 = 200.0$, $\tau_1 = 200.0$, $\bar{\varepsilon} = 10.0$, $r_{\max} = 100.0$, and $r_{\min} = 20.0$ mm. Those of the air-conditioning machine room recognition were $r_1 = 20.0$, $r_2 = 200.0$, $\tau_1 = 200.0$, $\bar{\varepsilon} = 10.0$, $r_{\max} = 150.0$, and $r_{\min} = 50.0$ mm.

The total recognition process took 4434 sec (the oil rig) and 1896 sec (the air-conditioning machine room), respectively, using a PC (Core-i7). The most time-consuming process of the algorithm was the one of extracting points of piping system (M1). The difference in time of the recognition process in both experiments was mainly caused by the one of the extracting points of piping system (M1). It took 3705 sec and 1220 sec, respectively. Because the structure of the oil rig is more complicated than the one of the air-condition room, more number of regions had to be extracted in the region-growing in case of the oil rig. As a result, more calculation in the oil rig was needed compared with the one in the air-conditioning machine room.

The final recognition results of the cylinders fitting to the straight pipes and those of the connecting parts are shown in Fig.7(b) and Fig.8(b).

The recognition accuracies of the straight pipes and the connecting parts are also shown in Table 1 and Table 2, respectively. The recognition rate of the straight pipe was about 87%~88%, that of elbows was about 77%~79% and that of junctions was over 75%. When being compared with the recognition rates of connecting parts and the calculation time of the scanned data of the oil rig in our former research [1], the rate of elbows was improved from 59.6% to 79.6%, and that of junctions was improved from 46.1% to 75.0%. The calculation time was improved from 6311 sec for about 1,720,000 scanned points to 4434 sec for about 4,500,000 points.

On the other hand, comparative evaluation of these accuracies with the other studies is difficult because we could not find any other papers in which the recognition rates of the piping system were quantitatively verified. However, the recognition rates in some researches where simple primitive objects such as cylinders or planes were recognized from laser scanned data have about 87%~88% accuracies [14,15]. Considering the researches used higher density point clouds than ours, the recognition accuracies of the piping system by our algorithm are thought to be effective and plausible.

9 Conclusion

A new algorithm was proposed that can automatically recognize a piping system from laser scanned points of a plant. The points of piping systems could be extracted by normal based region-growing. The points on straight pipes could be recognized by the normal tensor, and the radii and positions of straight pipes could be recognized by cylinder fitting using the non-linear least square method. The connecting parts could be recognized by tracing axes of a piping system and fitting line-arc segments. The recognition rate was verified by large-scale points of two actual plants, and the results showed the potential effectiveness of the proposed

algorithm.

Acknowledgements

We wish to thank Research Institute for Science and Engineering, Leica Co., Ltd and Shinryo Co., Ltd for providing the laser scanned data sets. This research was financially supported by Japan Ministry of Education, Culture, Sports, Science and Technology Grant-in-Aid for *Scientific Research* (B) under the project No. 24360057.

References

- [1] Kawashima, K., 2011, Automatic Recognition of a Piping System from Large-scale Terrestrial Laser Scan Data, ISPRS Workshop Laser Scanning 2011, Submission-20.
- [2] Masuda, H., 2010, As-built 3D Modeling of Large Facilities Based on Interactive Feature Editing, Computer-Aided Design and Applications, Vol.7, No.3, pp.349-360.
- [3] Ikeda, K., Masuda, H., 2011, Robust Edge Detection and GPU-Based Smoothing for Extracting Surface Primitives from Range Images, Computer-Aided Design and Applications, Vol.8, No.4, pp.519-530.
- [4] Rabbani, T., Heuvel, F., 2004, 3d Industrial Reconstruction by Fitting CSG Models to a Combination of Images and Point Clouds, In Proceedings of ISPRS The International Archives of Photogrammetry, Remote Sensing and Spatial Information Sciences, Vol.35, No.B3, pp.7-12.
- [5] Aurelien, B., Raphaelle, C., Raphael, M., Guillaume, T., Samir, A., 2011, Reconstruction of Consistent 3D CAD Models from Point Cloud Using A Priori CAD Models, ISPRS Workshop Laser Scanning 2011, Submission-26.
- [6] Andrew, E. J., Regis, H., Jim, O., Martial, H., 1997, A System for Semi-automatic Modeling of Complex Environments, In Proceedings of IEEE International Conference on Recent Advances in 3-D Digital Imaging and Modeling, pp.213-220.
- [7] Yan, D. M., Wintz, J., Mourrain, B., Wang, W., Boudon, F., Godin, C., 2009, Efficient and Robust Branch Model Reconstruction from Laser Scanned Points, In Proceedings 11th IEEE International Conference on Computer-Aided Design and Computer Graphics.
- [8] Alexander, B., Rodelik, L., Massimo, M., 2010, SkelTre – Robust skelton extraction from imperfect point clouds, The Visual Computer, International Journey of Computer Graphics - Special issue on 3D Object Retrieval, Vol.26, No.10, pp.1283-1300.
- [9] Zhouwang, Y., Tae-wan, K., 2007, Moving Parabolic Approximation of Point Clouds, Computer-Aided Design, Vol.39, No.12, pp.1091-1112.
- [10] Qian, Y. Z., Ulrich, N., 2008, Fast and Extensible Building Modeling from Airborne LiDAR Data, Proceedings of the 16th ACM SIGSPATIAL International Conference on Advances in Geographic Information Systems, pp.1-8.

- [11] William, R., Klecka., 1980, Discriminant analysis, SAGE, Sage university papers series, pp.71.
- [12] Shakarji, C, M., 1998, Least-Squares Fitting Algorithms of the NIST Algorithm Testing System, Journal of Research of the National Institute of Standards and Technology, Vol.103, No.6, pp.633-641.
- [13] Bauer, U., Polthier, K., 2009, Generating parametric models of tubes from laser scans, Computer-Aided Design, Vol.41, No.10, pp.719-729.
- [14] Rasu, R, B., Martin, Z, C., Blodow, N., Beetz, M., 2008, Learning informative Point Classes for the Acquisition of Object Model Maps, In Proceedings of the 10th International International Conference on Control, Animation, Robotics and Vision (ICARCV), pp.643-650.
- [15] Biegelbauer, G., Vincze, M., 2007, Efficient 3D Object Detection by Fitting Superquadrics to Range Image Data for Robot's Object Manipulation, IEEE International Conference on Robotics and Automation, pp.1086-1091.

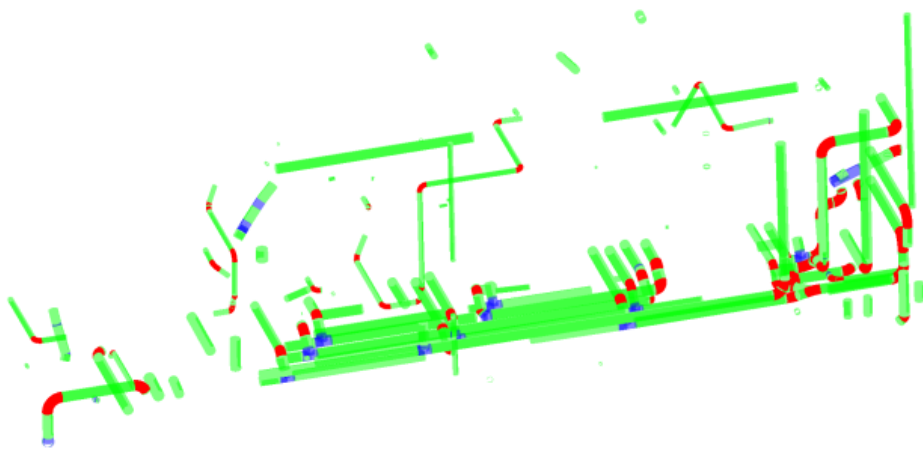
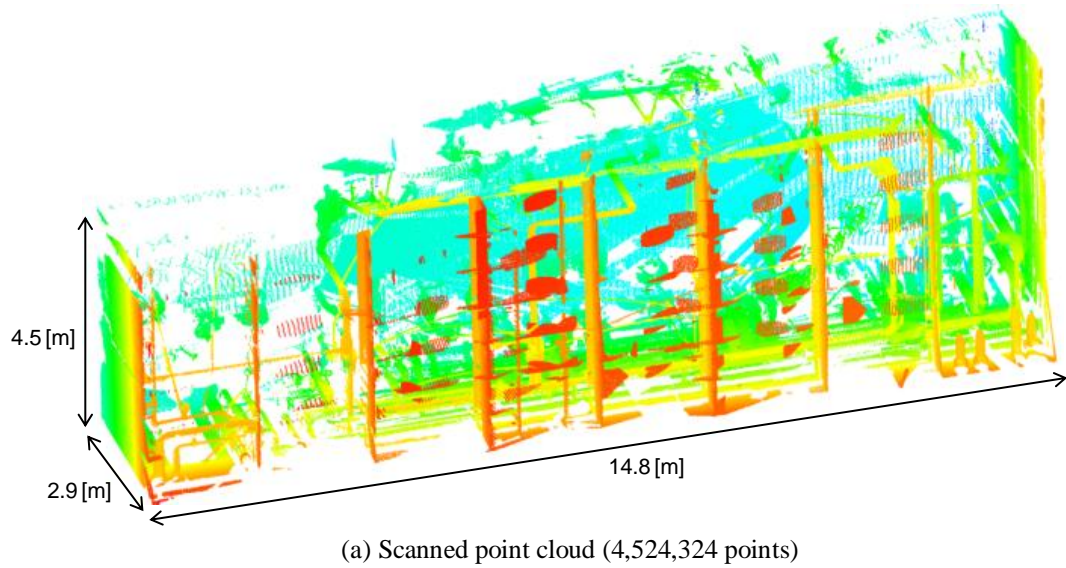


Figure.7 Recognition result of piping system of an oil rig

Table.1 Accuracy of piping system recognition of an oil rig

(a) Pipe

		Result of automatic recognition			
		Pipe	Not recognized	Total	Recognition rate [%]
True class	Pipe	95	13	108	88.0
True class	Other	75	-	-	-
True class	Total	170	-	-	-

(b) Connecting parts

		Result of automatic recognition					False recognition	
		Elbow	Junction	Not recognized	Total	Recognition rate [%]	False Negative [%]	False Positive [%]
True class	Elbow	43	0	11	54	79.6	20.4	27.8
True class	Junction	3	12	1	16	75.0	25.0	75.0
True class	Others	15	12	-	-	-	-	-
True class	Total	61	24	-	-	-	-	-

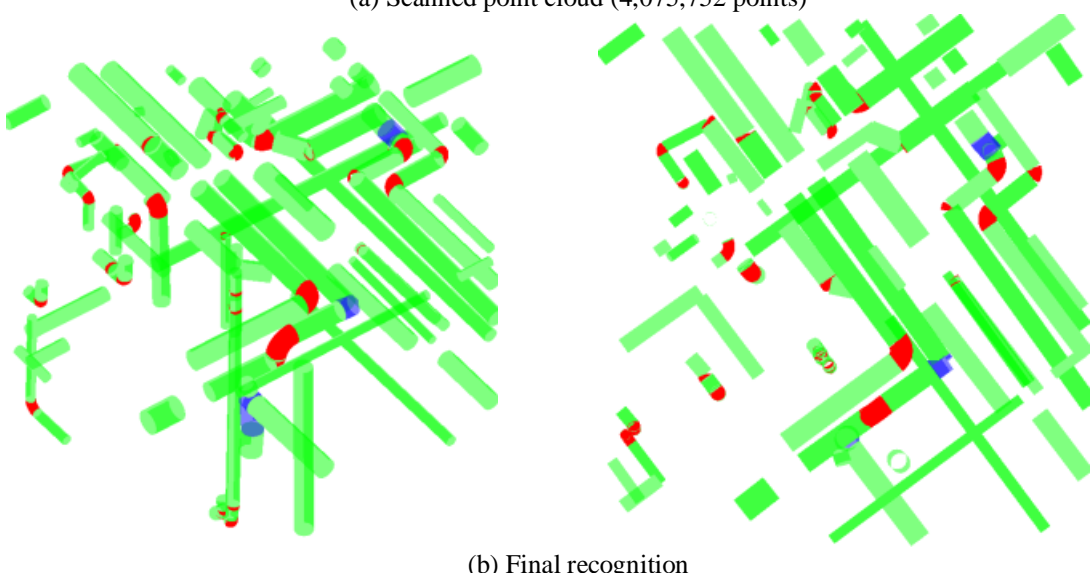
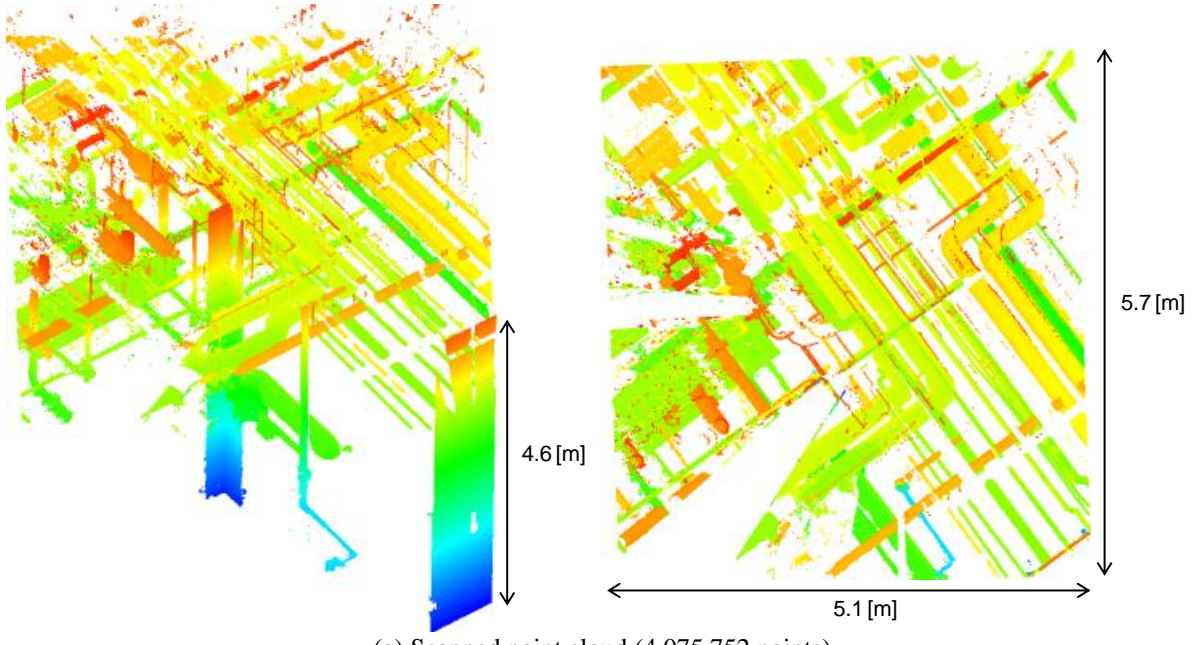


Figure.8 Recognition result of piping system of an air-conditioning machine room

Table.2 Accuracy of piping system recognition of an air-conditioning machine room

(a) Pipe

		Result of automatic recognition			
		Pipe	Not recognized	Total	Recognition rate [%]
True class	Pipe	34	5	39	87.2
	Other	64	-	-	-
	Total	98	-	-	-

(b) Connecting parts

		Result of automatic recognition				False recognition		
		Elbow	Junction	Not recognized	Total	Recognition rate [%]	False Negative [%]	False Positive [%]
True class	Elbow	17	2	3	22	77.2	22.8	81.8
	Junction	0	1	0	1	100.0	0.0	200.0
	Others	18	0	-	-	-	-	-
	Total	35	3	-	-	-	-	-